Heliyon 10 (2024) e36408

Contents lists available at ScienceDirect

Heliyon

journal homepage: www.cell.com/heliyon

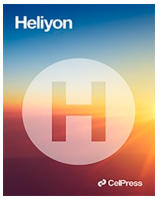

Research article

# A new route to the synthesis of 2-hydrazolyl-4-thiazolidinone hybrids, evaluation of α-glucosidase inhibitory activity and molecular modeling insights

Saghi Sepehri [a,b,*], Ghazaleh Farhadi [c], Maryam Maghbul [d], Farough Nasiri [d,**], Mohammad Ali Faramarzi [e], Karim Mahnam [f], Somayeh Mojtabavi [e], Mohammad Mahdavi [g,***], Zhaleh Moharrami Oranj [d]

[a] *Pharmaceutical Sciences Research Center, Ardabil University of Medical Sciences, Ardabil, Iran*
[b] *Department of Medicinal Chemistry, School of Pharmacy, Ardabil University of Medical Sciences, Ardabil, Iran*
[c] *Students Research Committee, School of Pharmacy, Ardabil University of Medical Sciences, Ardabil, Iran*
[d] *Department of Applied Chemistry, University of Mohaghegh Ardabili, Ardabil, Iran*
[e] *Department of Pharmaceutical Biotechnology, Faculty of Pharmacy, Tehran University of Medical Sciences, Tehran, Iran*
[f] *Department of Biology, Faculty of Sciences, Shahrekord University, Shahrekord, Iran*
[g] *Endocrinology and Metabolism Research Center, Endocrinology and Metabolism Clinical Sciences Institute, Tehran University of Medical Sciences, Tehran, Iran*

ARTICLE INFO

*Keywords:*
Diabetes
α-glucosidase
*In silico* study
Molecular dynamics simulations
Docking study

ABSTRACT

One of the multifactorial worldwide health syndromes is diabetes mellitus which is increasing at a disturbing rate. The inhibition of α-glucosidase, an enzyme that catalyzes starch hydrolysis in the intestine, is one helpful therapeutic approach for controlling hyperglycemia related to type-2 diabetes. To discover α-glucosidase inhibitors, some 2-hydrazolyl-4-thiazolidinone hybrids (**3a-e**) were synthesized from new one-pot reaction procedures. Next, their chemical structures were confirmed by $^{1}$H NMR, $^{13}$C NMR, and FT-IR spectra, and elemental analysis technique. Then, the α-glucosidase inhibitory activity of the titled compounds was evaluated. Among them, derivatives **3b** and **3c** revealed the highest activity against α-glucosidase compared to acarbose as a drug. Enzyme kinetic studies of the most active derivative (**3b**) indicated a competitive inhibition. Finally, molecular modeling studies were accomplished to describe vital interactions of the most potent compounds (**3b** and **3c**) with the α-glucosidase enzyme.

## 1. Introduction

One of the risk factors for Alzheimer's, cognitive decline, and cardiovascular diseases is diabetes [1]. Type 2 diabetes mellitus (T2DM) is known as one of the most widespread health problems in the world involving about 462 million patients equivalent to 6.28 % of the world's people and more than 1 million deaths per year [2,3].

* Corresponding author. Pharmaceutical Sciences Research Center, Ardabil University of Medical Sciences, Ardabil, Iran.
** Corresponding author.
*** Corresponding author.
*E-mail addresses:* saghisepehridr@gmail.com, s.sepehri@arums.ac.ir (S. Sepehri), nasiri@uma.ac.ir (F. Nasiri), momahdavi@tums.ac.ir (M. Mahdavi).

https://doi.org/10.1016/j.heliyon.2024.e36408
Received 25 June 2024; Received in revised form 10 August 2024; Accepted 14 August 2024
Available online 18 August 2024

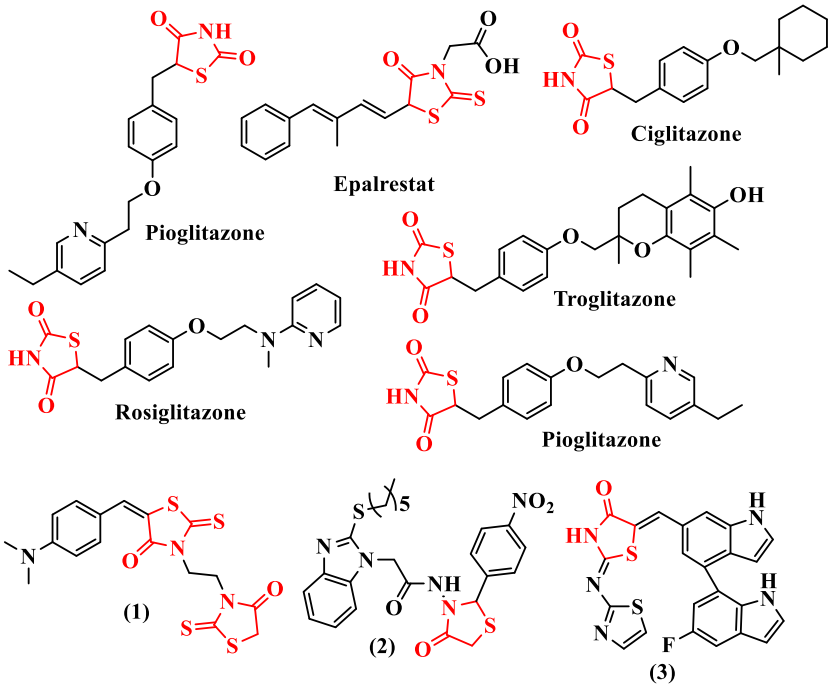


**Fig. 1.** Drugs and reported synthetic α-glucosidase inhibitors.

Diabetes is commonly treated with insulin and oral antidiabetic drugs like 4-thiazolidinones, biguanides, sulphonylureas, α-glucosidase and *β*-glucosidase inhibitors [4]. α-Glucosidase (EC.3.2.1.20) is an enzyme found at the intestine's brush border that breaks down oligosaccharides, trisaccharides, and disaccharides into monosaccharides [5]. α-Glucosidase inhibitors were used in the 1970s and the first α-glucosidase inhibitors for diabetes therapy were approved in the 1990s [6]. An FDA-approved α-glucosidase inhibitor titled acarbose, is used orally to regulate blood sugar levels. Other FDA-approved α-glucosidase inhibitors are voglibose, nojirimycin, and miglitol [7,8]. These drugs show serious side effects for example gastrointestinal disturbances like diarrhea, abdominal distension, and flatulence. Furthermore, numerous small molecules of α-glucosidase inhibitors have been synthesized with imidazole, quinazolinone, isatin, pyrazoles, xanthone, and azole scaffolds [9].

4-Thiazolidinones are among the most extensively studied organic compounds and their derivatives have been shown diversity of biological activities such as anti-diabetics, anti-bacterial [10], anti-fungal [11], antioxidant [12], anti-inflammatory [13], and anti-tuberculosis [14]. In nature, penicillin derivatives have the thiazolidine ring which was the first identification of medicinal features of this scaffold [15,16]. Thiazolidinone analogues are used also as α-glucosidase inhibitors [17].

Thiazolidinone-based derivatives showed capacity as single- and multi-targeted agents for regulatory hyperglycemia in T2DM [18]. In specific, the 2,4-thiazolidindione pioglitazone is a famous oral drug applied for the administration of T2DM, and the only drug approved to treat diabetic neuropathy is epalrestat, a 2-thioxo-4-thiazolidinone analogue [19]. Moreover, thiazolidinones, such as ciglitazone, rosiglitazone, troglitazone, and pioglitazone, are insulin-sensitizing drugs beneficial in the diagnosis of T2DM. Unfortunately, all drugs due to having high side effects were withdrawn from the market [20].

There are some studies on thiazolidinone derivatives as α-glucosidase inhibitors. For example, Azam et al. assessed the various thiazolidinones against α-glucosidase. Compound **1** (Fig. 1) exhibited potent α-glucosidase inhibition compared to acarbose [21]. Khan et al. reported a series of 2-mercaptobenzimidazole-based 1,3-thiazolidin-4-ones as α-glucosidase inhibitors. Compound **2** (Fig. 1) displayed excellent activity [22]. Khan et al. evaluated thiazolidinone-based indole derivatives against α-glucosidase activity. Analogue **3** (Fig. 1) exhibited a few folds better inhibitory activity than acarbose [23]. Yakaiah Chintala et al. described the α-glucosidase inhibitory activity of triazole linked to thiazolidinedione. Compound **4** (Fig. 1) revealed potent α-glucosidase inhibition [24].

According to the high activity of the thiazolidinone derivatives as α-glucosidase inhibitors, in the current study, a series of 2-hydrazolyl-4-thiazolidinone hybrids with a new synthesis route and more yield were provided and evaluated against α-glucosidase enzyme. Furthermore, *in vitro* kinetic analysis and *in silico* investigations were carried out to clarify the interactions between these derivatives and the α-glucosidase active site.

## 2. Materials and methods

### 2.1. General

Alkylidene or benzylidene hydrazines were prepared from the reaction between aldehydes and hydrazine hydrate, based on the reported procedure [25]. Other starting materials and solvents were obtained from Merck (Germany) and were used without further purification. Progress of the reaction was monitored by analytical thin-layer chromatography (TLC) on silica gel 60 $F_{254}$ aluminum-backed silica plates (Merck). Melting points (uncorrected) were measured with a Stuart SMP-3 apparatus. Elemental analysis (C, H, N, and S) was performed using a CHNS-923 LECO analyzer (USA). FT-IR spectra of compounds were measured with an FT-IR PerkinElmer RXI. NMR spectra were reported on a Bruker 250 MHz (250.1 MHz for $^1$H and 62.9 MHz for $^{13}$C) with $CDCl_3$ as the solvent. Chemical shifts are given in ppm ($\delta$) relative to internal TMS, and coupling constants ($J$) are reported in Hertz (Hz).

### 2.2. Synthesis

General procedure for the preparation of alkyl 2-(2-(arylidenehydrazino)-4-oxo-3-phenylthiazolidin-5-ylidene)acetates (3a-e), exemplified by 3a.

A mixture of 2-(4-nitrophenyl)ethen-1-amine **1a** (2 mmol) and phenyl isothiocyanate (2 mmol) in absolute ethanol (5 mL) was stirred for 15 min at room temperature. After that, diethyl acetylenedicarboxylate **2a** (2 mmol) was added to the reaction mixture, and the mixture was stirred for 14 h at room temperature. Then, the light-yellow precipitate was filtered and washed with a mixture of *n*-hexane/ethyl acetate to produce pure product **3a**.

#### 2.2.1. (Z)-Ethyl-2-(2-((4-nitrobenzylidene)hydrazono)-4-oxo-3-phenylthiazolidin-5-ylidene) acetate (3a)

Yellow powder, yield: 0.62 g (73 %), mp: 208–209 °C, FT-IR (KBr, $cm^{-1}$): 1725 (C=O), 1692 (C=O), 1602 (C=N). $^1$H NMR (250.1 MHz, $CDCl_3$): $\delta$ ppm 1.35 (3H, t, $^3J_{HH}$ = 7.0 Hz, $CH_3$), 4.36 (2H, q, $^3J_{HH}$ = 7.0 Hz, $OCH_2$), 7.00 (1H, s, CH), 7.40–7.58 (5H, m, Ar–H), 7.92 (2H, d, $^3J_{HH}$ = 8.8 Hz, Ar–H), 8.32 (2H, d, $^3J_{HH}$ = 8.8 Hz, Ar–H), 8.57 (1H, s, CH). $^{13}$C NMR (62.9 MHz, $CDCl_3$): $\delta$ ppm 14.2 ($CH_3$), 62.0 ($OCH_2$), 117.5 (CH), 124.0 (2CH), 127.6 (2CH), 128.9 (2CH), 129.4 (3CH), 133.7 (C), 139.5 (C), 140.6 (C), 149.2 (C), 157.6 (CH), 163.3 (C), 164.6 (C), 166.0 (C). Anal. Calc. for $C_{20}H_{16}N_4O_5S$ (424.08): C, 56.60; H, 3.80; N, 13.20; S: 7.55 found: C, 56.94; H, 3.92; N, 13.49; S: 7.76 %.

#### 2.2.2. (Z)-Methyl-2-(2-((4-nitrobenzylidene)hydrazono)-4-oxo-3-phenylthiazolidin-5-ylidene) acetate (3b)

Yellow powder, yield: 0.56 g (68 %), mp: 199–200 °C, FT-IR (KBr, $cm^{-1}$): 1723 (C=O), 1696 (C=O), 1602 (C=N). $^1$H NMR (250.1 MHz, $CDCl_3$): $\delta$ ppm 3.92 (3H, s, $OCH_3$), 7.03 (1H, s, CH), 7.40–7.58 (5H, m, Ar–H), 7.94 (2H, d, $^3J_{HH}$ = 8.8 Hz, Ar–H), 8.27 (2H, d, $^3J_{HH}$ = 8.8 Hz, Ar–H), 8.41 (1H, s, CH). $^{13}$C NMR (62.9 MHz, $CDCl_3$): $\delta$ ppm 52.7 ($OCH_3$), 117.1 (CH), 124.0 (2CH), 127.6 (2CH), 129.0 (2CH), 129.4 (3CH), 132.3 (C), 139.2 (C), 141.5 (C), 143.8 (C), 157.7 (CH), 161.0 (C), 161.2 (C), 166.5 (C). Anal. Calc. for $C_{19}H_{14}N_4O_5S$ (410.40): C, 55.61; H, 3.44; N, 13.65; S: 7.81 found: C, 55.24; H, 3.65; N, 13.89; S: 7.66 %.

#### 2.2.3. Ethyl (Z)-2-((E)-2-(((1E,2E)-3-(2-nitrophenyl)allylidene)hydrazono)-4-oxo-3-phenylthiazolidin-5-ylidene) acetate (3c)

Yellow powder, yield:0.58 g (64 %), mp: 200–201 °C, FT-IR (KBr, $cm^{-1}$): 1727 (C=O), 1696 (C=O), 1601 (C=N). $^1$H NMR (250.1 MHz, $CDCl_3$): $\delta$ ppm 1.37 (3H, t, $^3J_{HH}$ = 7.3 Hz, $CH_3$), 4.34 (2H, q, $^3J_{HH}$ = 7.3 Hz, $OCH_2$), 6.98 (1H, s, CH), 6.93–7.55 (8H, m, Ar–H and 2CH), 7.66 (1H, t, $^3J_{HH}$ = 8.0 Hz Ar–H), 7.74 (1H, m, Ar–H), 8.00 (1H, d, $^3J_{HH}$ = 8.3 Hz, Ar–H), 8.19 (1H, d, $^3J_{HH}$ = 9.7 Hz, CH). $^{13}$C NMR (62.9 MHz, $CDCl_3$): $\delta$ ppm 14.2 ($CH_3$), 61.7 ($CH_2$), 117.2 (CH), 125.0 (CH), 127.6 (2CH), 129.1 (CH), 129.4 (CH), 129.9 (3CH), 131.3 (C), 133.4 (CH), 133.7 (CH), 136.6 (C), 136.8 (CH), 140.6 (C), 147.9 (C), 161.2 (C), 161.3 (C), 164.7 (C), 165.9 (C). Anal. Calc. for $C_{22}H_{18}N_4O_5S$ (450.47): C, 58.66; H, 4.03; N, 12.44; S: 7.12 found: C, 58.35; H, 3.85; N, 12.75; S: 7.28 %.

#### 2.2.4. (Z)-Methyl-2-(2-((4-cholorobenzylidene) hydrazono)-4-oxo-3-phenylthiazolidin-5-ylidene) acetate (3d)

Yellow powder, yield: 0.60 g (75 %), mp: 207–208 °C, FT-IR (KBr, $cm^{-1}$): 1720 (C=O), 1704 (C=O), 1613 (C=N). $^1$H NMR (250.1 MHz, $CDCl_3$): $\delta$ ppm 3.90 (3H, s, $OCH_3$), 6.98 (1H, s, CH), 7.25–7.86 (9H, m, Ar–H), 8.30 (1H, s, CH). $^{13}$C NMR (62.9 MHz, $CDCl_3$): $\delta$ ppm 52.6 ($OCH_3$), 116.5 (CH), 127.6 (2CH), 129.1 (2CH), 129.3 (CH), 129.4 (2CH). 129.6 (2CH), 132.5 (C), 133.8 (C), 137.3 (C), 141.4 (C), 159.0 (CH), 161.1 (C), 164.6 (C), 166.5 (C). Anal. Calc. for $C_{19}H_{14}ClN_3O_3S$ (399.85): C, 57.07; H, 3.53; N, 10.51; S: 8.02 found: C, 57.38; H, 3.36; N, 10.25; S: 7.73 %.

#### 2.2.5. Ethyl (Z)-2-((E)-2-(((E)-benzylidene)hydrazono)-4-oxo-3-phenylthiazolidin-5-ylidene)acetate (3e)

Yellow powder, yield: 0.38 g (50 %), mp: 223–225 °C, FT-IR (KBr, $cm^{-1}$): 1717 (C=O), 1688 (C=O), 1611 (C=N). $^1$H NMR (250.1 MHz, $CDCl_3$): $\delta$ ppm 1.38 (3H, t, $^3J_{HH}$ = 7.0 Hz, $CH_3$), 4.36 (2H, q, $^3J_{HH}$ = 7.0 Hz, $OCH_2$), 6.99 (1H, s, CH), 7.41–7.55 (8H, m, Ar–H), 7.78 (2H, d, $^3J_{HH}$ = 7.3 Hz, Ar–H), 8.36 (1H, s, CH). $^{13}$C NMR (62.9 MHz, $CDCl_3$): $\delta$ ppm 13.4 ($CH_3$), 60.9 ($OCH_2$), 116.0 (CH), 126.5 (C), 126.9 (2CH), 127.7 (2CH), 128.0 (2CH), 128.6 (3CH), 130.5 (CH), 133.0 (C), 140.5 (C), 159.5 (CH), 160.1 (C), 164.0 (C), 165.3 (C). Anal. Calc. for $C_{20}H_{17}N_3O_3S$ (379.43): C, 63.31; H, 4.52; N, 11.07; S: 8.45 found: C, 63.65; H, 4.41; N, 11.34; S: 8.26 %.

### 2.3. α-Glucosidase inhibition assay

The inhibitory activity of 2-hydrazolyl-4-thiazolidinone hybrids was evaluated on the α-glucosidase enzyme according to the

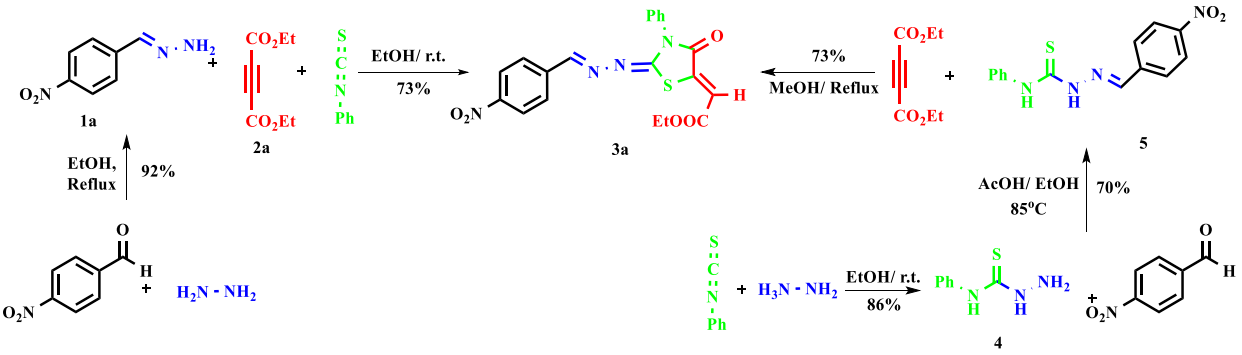


**Scheme 1.** Synthesis of 2-hydrazolyl-4-thiazolidinone **3a** via two routes - Benmohammed et al.'s 2014 [31] method (right) and our method (left).

previous procedure [26]. The *Saccharomyces cerevisiae* form of the α-glucosidase enzyme (EC 3.2.1.20) (purchased from Sigma-Aldrich) (20 U/mg) and *p*-nitrophenyl glucopyranoside (*p*NPG) as substrate were ready in the buffer of potassium phosphate (pH 6.8, 50 mM). After that, derivatives were dissolved in DMSO (10 % final concentration). The reaction mixture was added to the 96-well plates (including enzyme buffer (20 μL, 20 U/mg), potassium phosphate buffer (135 μL), and derivatives (20 μL)). Then, the mixture was incubated at 37 °C for 10 min. In the next step, incubation continued after the addition of the substrate (25 μL, 4 mM) at 37 °C for 20 min. Finally, a yellow color was produced due to the presence of the privation of *p*-nitrophenol. After that, the absorbance of compounds was recorded at 405 nm by using a spectrophotometer (Gen5, Power wave xs2, BioTek, America). DMSO (10 % final concentration) as negative control and acarbose as positive control were used. The percentage of enzyme inhibition for each compound was calculated by using the following formula:

$$\% \text{ Inhibition} = [\text{-Abs control Abs sample})/\text{Abs control}] \times 100$$

$IC_{50}$ values were calculated from a non-linear regression curve using the Logit method. All investigations were performed three times.

### 2.4. Enzyme kinetic studies

Enzyme kinetic studies were carried out on derivative **3c**, the most potent derivative recognized with the highest $IC_{50}$, against α-glucosidase activity. It was performed in the presence and absence of derivative **3c** at diverse concentrations (0, 43.5, 87.0, and 174.0 μM) with varied concentrations of *p*-nitrophenyl *α*-D-glucopyranoside (1–16 mM) as substrate. The enzyme kinetic methodology was similar to the procedure performed in the previous research [5].

### 2.5. Molecular docking study

The docking studies of the compounds into the isomaltase of *Saccharomyces cerevisiae* binding site were performed by software Autodock 4.2 [27]. The crystal structure of isomaltase of *Saccharomyces cerevisiae* (PDB code 3A4A) was reached from the protein data bank (PDB). The docking methodology was similar to the procedure of docking in the previous research [5].

### 2.6. Molecular dynamics simulations study

Molecular dynamics simulations (MD) was carried out via the GROMACS V4.5.5 computational package. MD methodology of derivatives was similar to the procedure of MD in the previous article [5].

### 2.7. Binding free energy analyses

Binding free energy was calculated for derivatives by the g_mmpbsa tool. This tool uses the MM/PBSA method to calculate binding free energy derivatives. MM/PBSA methodology of derivatives was similar to the procedure of MM/PBSA in the previous article [28].

## 3. Results and discussion

### 3.1. Chemistry

The synthesis of hydrazolyl-4-thiazolidinone hybrids with various biological activities has attracted the attention of researchers [29,30]. The described procedures for synthesizing these derivatives need several stages, and thiosemic carbazide derivatives are usually the key intermediates in these methods [29,31]. For example, highly functionalized thiazolidinone **3a** was synthesized by

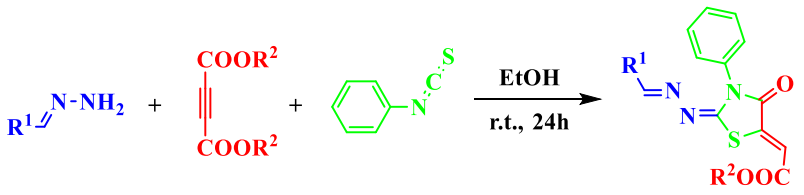


1 2 3

| Compound: | 3a | 3b | 3c | 3d | 3e |
|---|---|---|---|---|---|
| $R^1$: | 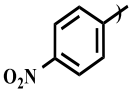 | 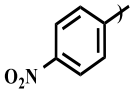 | 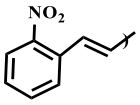 | 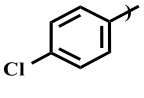 |  |
| $R^2$: | Et | Me | Et | Me | Et |
| Isolated yield% | 73 | 68 | 64 | 75 | 50 |

**Scheme 2.** The one-pot reaction between functionalized benzylidene/alkylidene hydrazines and phenyl isothiocyanate in the presence of dialkyl acetylenedicarboxylates.

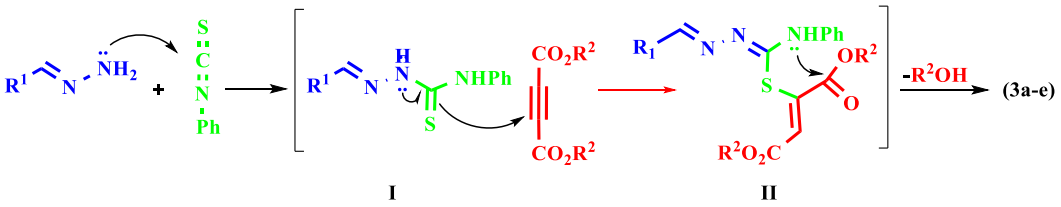


I II

**Scheme 3.** The proposed mechanism for the synthesis of 2-hydrazolyl-4-thiazolidinone derivatives (**3a-e**).

Benmohammad et al. [31] in three stages, achieving an overall yield of 44 %. This approach provided thiosemicarbazide derivatives **4** and **5** as intermediates. We suggested a different pathway to synthesize **3a** that could be a one-pot reaction involving benzylidene hydrazine **1a** and phenylisothiocyanate, in the presence of diethyl acetylenedicarboxylate **2a** (Scheme 1). Initially, we produced functionalized benzylidene hydrazine **1a** from the reaction of 4-nitobenzaldehyde and hydrazinehydrate, following the optimal conditions cited in previous studies [25]. Subsequently, we synthesized compound **3a** via a one-pot reaction between benzylidene hydrazine **1a** and phenyl isothiocyanate, with diethylacetylenedicarboxylate **2a** present. This method allowed us to reduce the synthesis steps to two steps and enhance the overall yield by approximately 67 % (Scheme 1).

In the current work, we report a facile synthesis of functionalized hydrazolyl-4-thiazolidinone derivatives (**3a-e**) through a one-pot reaction between functionalized benzylidene/alkylidene hydrazines **1** and phenyl isothiocyanate in the presence of dialkylacetylenedicarboxylates **2**.

Functionalized thiazolidine-4-one derivatives **3**, including two critical pharmacophores thiazolidinedin-4-one and imino/hydrazine groups, were synthesized by the one-pot reaction between functionalized benzylidene/alkylidene hydrazines **1** and dialkyl acetylenedicarboxylates **2** in the presence of phenylisothiocyanate. The first step of the synthesis included the preparation of benzylidene hydrazines **1** from the condensation reaction between hydrazine hydrate with substituted aldehydes, according to the literature [25]. Next, a one-pot reaction between benzylidene/alkylidene hydrazines **1** and dialkyl acetylenedicarboxylates **2** in the presence of phenylisothiocyanat produced hydrazinyl-4-thiazolidinone derivatives (**3a-e**) in good yields (Scheme 2).

The synthetic methodology employed was straightforward, and the resulting compounds were efficiently purified by simple washing with a *n*-hexane/ethyl acetate solvent system. The high purity of the isolated compounds was confirmed by TLC, sharp melting points, and corroborative elemental analysis data (see Experimental). The structures of compounds **3a** and **3c** were assigned by comparison of their spectroscopic data with literature precedents [31]. The structures of the remaining new compounds were established through comprehensive spectroscopic analysis, including $^1$H NMR, $^{13}$C NMR, and FT-IR spectroscopy, as well as elemental analysis. The results of elemental analysis for all products were in good agreement with the calculated values. FT-IR spectra exhibited characteristic peaks at approximately 3057–3070 cm$^{-1}$ (aromatic C–H), 2854–2926 cm$^{-1}$ (aliphatic C–H), 1717–1727 cm$^{-1}$ (ester carbonyl), 1688–1704 cm$^{-1}$ (thiazolidinone carbonyl), and 1601–1613 cm$^{-1}$ (-C=N-). $^1$H NMR spectra revealed signals at $\delta$ 8.19–8.57

**Table 1**
Evaluation of α-glucosidase inhibitory activity of compounds (**3a-e**).

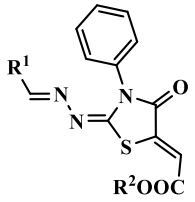

| Compound | $R^1$ | $R^2$ | $IC_{50}$ (μM) |
|---|---|---|---|
| **3a** | 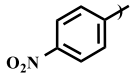 | Et | >750 |
| **3b** | 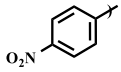 | Me | 215.4 ± 0.9 |
| **3c** | 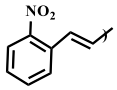 | Et | 174.0 ± 0.4 |
| **3d** | 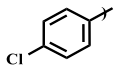 | Me | 488.9 ± 1.6 |
| **3e** |  | Et | >750 |
| **Acarbose** | – | - | 750 ± 2.0 |

ppm (aldimine –HC=N- proton), 6.98–7.03 ppm (vinylic = *CH*$CO_2$R proton), 4.34–4.36 ppm (ester $CH_2$ in **3a**, **3c**, and **3e**), 3.90–3.92 ppm (ester $CH_3$ in **3b** and **3d**), 1.35–1.38 ppm (ester $CH_3$ in **3a**, **3c**, and **3e**), and 6.93–8.32 ppm (aromatic protons). $^{13}$C NMR spectra exhibited resonances at $\delta$ 13.4–62.0 ppm (ester aliphatic carbons), 116.0–117.5 ppm (vinylic = *CH*$CO_2$R carbon), 157.6–161.2 ppm (aldimine –HC=N- carbon), 161.0–166.5 ppm (carbonyl and imino carbon of thiazolidinone ring and ester carbonyl), and 124.0–149.2 ppm (aromatic carbons and C-5 of thiazolidinone ring).

The reaction mechanism being proposed is depicted in Scheme 3. The process begins with the addition of benzylidene/alkylidene hydrazines to phenylisothiocyanate, resulting in the formation of an intermediate known as **I**. This intermediate then proceeds to react with dialkyl acetylenedicarboxylate, leading to the production of intermediates referred to as **II**. Following this, these intermediates undergo a process of intramolecular cyclization, culminating in the production of 2-hydrazolyl-4-thiazolidinone derivatives **3**, as shown in Scheme 3.

### *3.2. α-Glucosidase inhibition assay*

To evaluate the inhibitory activity of the derivatives (**3a-e**), the α-glucosidase enzyme (*Saccharomyces cerevisiae* form) was applied. Based on the findings, some of the evaluated compounds ($IC_{50}$ = 174–488 μM) were more potent toward the acarbose ($IC_{50}$ = 750 μM) (Table 1). Among compounds, the derivative **3c** was the most potent compound with $IC_{50}$ values equal to 174 μM.

The assay results showed that the position and the nature of substituents on the phenyl ring of hydrazolyl moiety play an important role against the α-glucosidase. Compound **3c**, the most potent derivative, was bearing *ortho*-nitrophenyl-allylidene in hydrazolyl moiety. Shortening the length of the liker between the phenyl ring and hydrazolyl moiety and moving the nitro group from the *ortho* to *para* position decreased inhibitory activity. For example, compound **3c** ($IC_{50}$ = 174.0 μM) showed higher inhibitory activity than compounds **3b** ($IC_{50}$ = 215.4 μM), **3a** ($IC_{50}$ > 750 μM), and **3d** ($IC_{50}$ = 488.9 μM). Changing the nitro group on the benzyl ring with hydrogen or chlorine atoms **3e** ($IC_{50}$ > 750 μM) and **3d** ($IC_{50}$ = 488.9 μM) dramatically decreased activity. It seems that the presence of diverse groups at the *para* position of the phenyl ring of hydrazolyl moiety was effective against α-glucosidase.

Likewise, the presence of an electron-withdrawing and hydrophilic substituent on the phenyl ring increased inhibitory activity. Additionally, the introduction of ethyl ester in thiazolidinone moiety compared to methyl ester decreased inhibitory activity, which might be due to increased lipophilic features at this position [32–34].

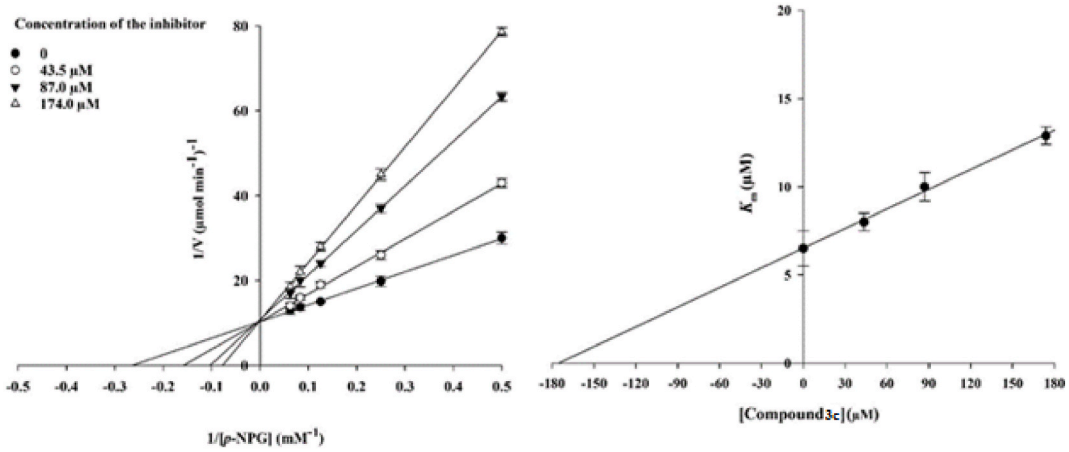


**Fig. 2.** Kinetics of α-glucosidase inhibition by derivative **3c**. (a) The Lineweaver-Burk plot in the presence and absence of diverse concentrations of the derivative **3c**; (b) The secondary plot between $K_m$ and various concentrations of the derivative **3c**.

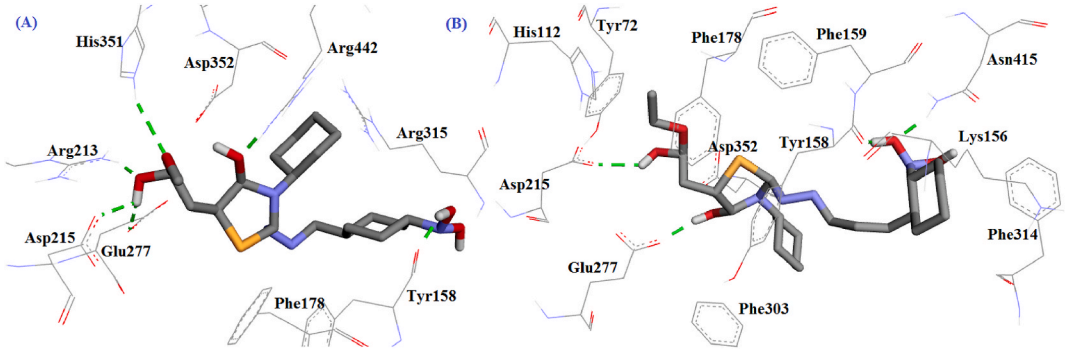


**Fig. 3.** Binding mode of (**A**) derivative **3b** and (**B**) derivative **3c** in α-glucosidase active site.

### 3.3. Enzyme kinetic studies

The Lineweaver-Burk plot exhibited that $V_{max}$ remained unchanged and the $K_m$ slowly increased with increasing inhibitor concentration representing a competitive inhibition (Fig. 2a). The findings exhibited that **3c** competes with the substrate for binding to the active site. Moreover, the plot of the $K_m$ versus diverse concentrations of inhibitor provided a $K_i$ of 174.0 µM (Fig. 2b).

### 3.4. Molecular docking study

The screened derivatives based on the number and type of groups linked to the carboxylate moiety of the main scaffold, and positions of the functional group on the phenyl ring can inhibit α-glucosidase (Table 1). These derivatives were diverse in the kind and position of the substituted moieties (Table 1). Docking calculations of evaluated derivatives was done to achieve of estimated score docking and suitable interactions in active site enzyme. Validation of the docking methodology was carried out using a re-dock of native co-crystallized into the binding site of α-glucosidase. The docking protocol successfully restored the docked ligand alignment of the native co-crystallized with an RMSD equal to 1.32 Å.

Derivative **3c**, the most potent compound, showed appropriate interactions with the active site residues. Fig. 1 shows the interactions of the best docked conformation of **3c** with the active site residues. The oxygen atom of the nitro group of compound **3c** made two hydrogen bonds with Asn415 and Tyr158 residues. The carbonyl group in the ethyl ester of the compound showed a hydrogen bond with Asp215. The carbonyl group of thiazolidinone moiety also exhibited another hydrogen bond with Glu277. This derivative displayed hydrophobic interactions with Tyr316, Phe314, Phe159, Ser157, Lys156, Val216, Glu411, Gln353, Arg315, Tyr72, Asp69, Phe178, Gln182, His112, Asp352, Arg442, Phe303 (Fig. 3).

Compound **3b**, second rank after compound **3c**, showed hydrophobic interactions with Phe314, Glu411, Phe33, Tyr158, Arg315, Gln353, Phe178, Val216, Gln279, Asp352, Asp215, Glu277, Tyr72, Asp69 residues. This compound exhibited five hydrogen bonds with residues: the carbonyl group of the compound with Arg442, methyl ester of the ligand with His351, and three hydrogen bonds between the carbonyl group of the compound and Arg213, Asp215 and Glu277 (Fig. 3).

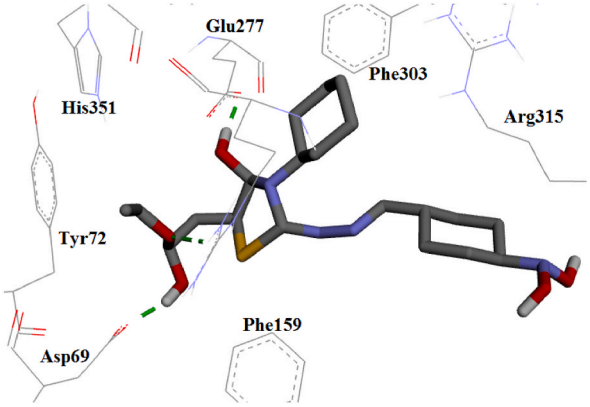


**Fig. 4.** Conformation of derivative **3a** in α-glucosidase active site.

Increasing the length of the linker between the hydrazolyl moiety and the phenyl ring affected the activity. Docking results exhibited that increasing the length of the linker and moving the nitro group from *para* to *ortho* position might lead to a conformation change in the active site [35–37]. That could be effective in inhibitory activity (compound **3b** ($IC_{50}$ = 215.4 μM) ($\Delta G_{binding}$ = −10.23 kcal/mol) *vs.* compound **3c** ($IC_{50}$ = 174.0 μM) ($\Delta G_{binding}$ = −11.61 kcal/mol)). Based on previous reports all almost residues that interacted with these compounds play an important role in the binding and inhibitory activity of compounds [5,9,38].

Comparison of the binding mode of acarbose as the drug and positive control in the active site [5] with compounds **3b** and **3c** showed that these two compounds formed hydrogen bonds and hydrophobic interactions with Tyr72, Phe314, Tyr158, Phe303, Asp352, Arg442, His112, and Asp215 similar to acarbose. Moreover, they showed more interactions than acarbose with residues. Thus, extra interactions can be important for binding, which these compounds were more potent compared to acarbose. Further studies showed that compounds with lower inhibitory activity *e.g.* **3a** have fewer interactions with the key residues of the active site than the most potent compounds (**3b** and **3c**) and acarbose.

Replacing methyl ester (compound **3b**) with the ethyl ester (compound **3a**) dramatically reduced the inhibitory effect. The weak activity of **3a** might be ascribed to a slight conformation change and dropping the establishment of hydrogen bonds and key hydrophobic interactions. It appears that extra hydrogen bonds hydrophobic interactions show a positive effect. Moreover, the ester of derivative **3a** made hydrogen bonds with Asp69, Arg442 and Glu277 (Fig. 4), while the ester moiety of compounds **3b** and **3c** made hydrogen bonds with Asp215, Glu277, Arg213 and His351 residues.

Replacement *para*-chlorophenyl ring of compound **3d** with the *para*-nitrophenyl ring of compound **3a** intensely decreased inhibitory activity. The differences between the groups along with the $\Delta G_{bind}$ values for compounds **3b** ($\Delta G_{bind}$ = −10.23 kcal/mol) and **3d** ($\Delta G_{bind}$ = −9.55 kcal/mol) may account for the differences between the inhibitory potency of these compounds. Moreover, compound **3b** showed lower hydrophobic features than compound **3d** (CLogP = 3.45 for **3b** *vs.* CLogP = 4.42 for **3d**). This may be attributed to the poor penetration ability of this compound to the outer membrane of the cell.

Un-substituted phenyl ring in comparison to the substituted phenyl ring showed lower inhibitory activity and free binding energy. In comparison to **3a** and **3e**, the un-substituted phenyl ring is inappropriate for the activity and caused a reduction of interaction with key residues. That caused a decrease in the formation of hydrogen bonds at the ester moiety and eliminated hydrogen bonds at the phenyl ring. Therefore, these interactions might be important for the stability of the compound at the active site.

From the structural differences of these compounds, assay findings, and their molecular docking study, it was observed that the compounds that have attachment groups in the *ortho* position over the aromatic ring have good interaction networks as well as inhibitory activities as compared to the compounds having either *para* attachment or without group. Similarly, a good inhibition mode was observed for most electronegative groups than less electronegative groups attached over the aromatic phenyl ring. Moreover, increasing the length of the linker of the phenyl ring to the hydrazolyl moiety changes the binding mode and the binding to amino acids.

The comparison of compounds showed that: (1) extra hydrogen bonds have a positive effect on α-glucosidase inhibition, (2) Asp215 and Glu277 residues are important for the formation of hydrogen bonds, (3) Tyr158, Asp352, Phe303, His112, and Phe178 residues are main for the hydrophobic interactions, (4) presence nitro group at *ortho* position is better than *para* position due to more hydrogen bond formation and appropriate orientation of the compound in the active site, (5) the formation of hydrogen bond between carbonyl group of hydrazolyl moiety and Glu277 is important for activity, (6) increasing the length of the linker of the phenyl ring to the hydrazolyl moiety have a positive effect on α-glucosidase inhibition. These findings are aligned with acarbose and previous reports [5, 39–41].

The active and moderately active compounds' binding modes were all oriented more or less in a similar fashion, which they were similar to the binding mode of acarbose, while in contrast, the least active compounds' binding modes were all oriented differently from the active ones and acarbose.

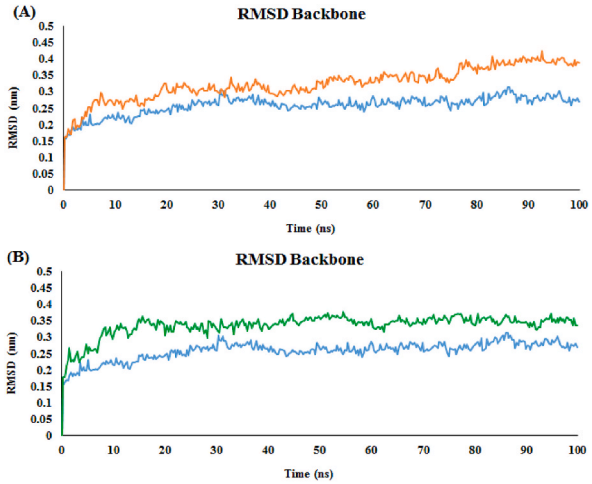


**Fig. 5.** RMSD backbone plot of the α-glucosidase backbone in complexed with acarbose (in blue) and (A) compound **3b** (in brown), (B) compound **3c** (in green) 100 ns of the MD simulation time.

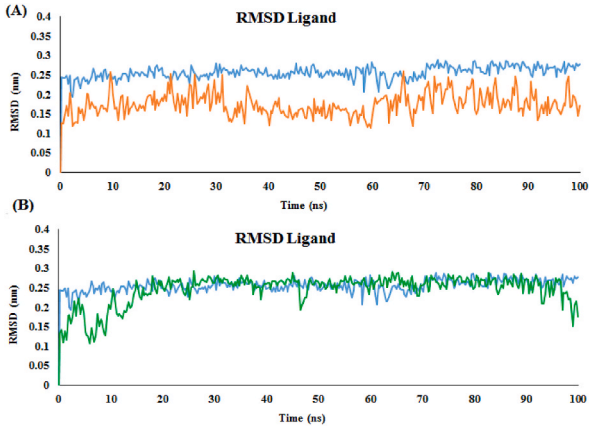


**Fig. 6.** RMSD ligand plot of the acarbose (in blue) and (A) compound **3b** (in brown), (B) compound **3c** (in green) 100 ns of the MD simulation time.

### *3.5. Molecular dynamics simulation study*

In the docking methodology, ligand-protein complex interactions are instant and potentially unstable. Therefore, molecular dynamics (MD) simulations is performed for the study of compound stability in the active site. It investigates the separate element motions and identifies the stability of the complex as a function of time more easily than experiments in the actual system [42].

### *3.6. Root mean square deviation (RMSD)*

The dynamic stabilities of all systems can reflect via root mean square deviations (RMSDs) for all heavy atoms of each ligand, backbone atoms of amino acids in the active site within 5 Å around the ligand, and all backbone atoms of the protein. The RMSDs of the two complexes compared to the acarbose complex are shown in Fig. 5. The blue line in Fig. 5 displays the acarbose-α-glucosidase complex. The RMSD plot of acarbose became overall stable after 12 ns and the RMSD average value was at about 2.5 Å. The RMSD plot of derivative **3b** also got an equilibration state after 12 ns with a higher RMSD value (>3 Å) (Fig. 5, brown line). However, The RMSD plot of derivative **3c** touched an equilibration state after 9 ns with an RMSD value equal to 3.5 Å (Fig. 5, green line).

Compound **3c** complexed α-glucosidase was stable after equilibrium. The compound **3b** exhibited diverse dynamics performances in the α-glucosidase active site. According to Fig. 5, the fluctuations of the RMSD plot were about 3.0 Å at the first 50 ns. Then, a sharp increase was detected and kept stable with average RMSD values of 4.0 Å until the end of the MD simulation. This showed that the conformation of derivative **3b** changes during simulation.

Likewise, the RMSD of molecules was also calculated separately (Fig. 6). The ligands **3c** and **3b** in the α-glucosidase enzyme exhibited a stable RMSD plot with small fluctuations of 2.5 and 2.0 Å, respectively. Based on the RMSD of ligand **3c**, a large fluctuation was not observed and it was very stable during the simulation similar to acarbose (Fig. 6). However, compound **3b** exhibited stability

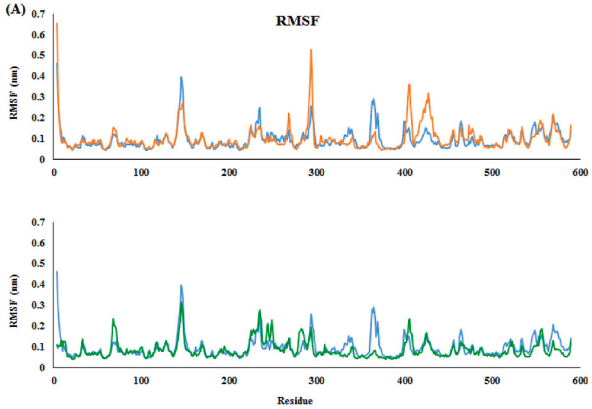


**Fig. 7.** RMSF plot of the α-glucosidase residue in complexed with acarbose (in blue) and compound **3c** (in green) and compound **3b** (in brown).

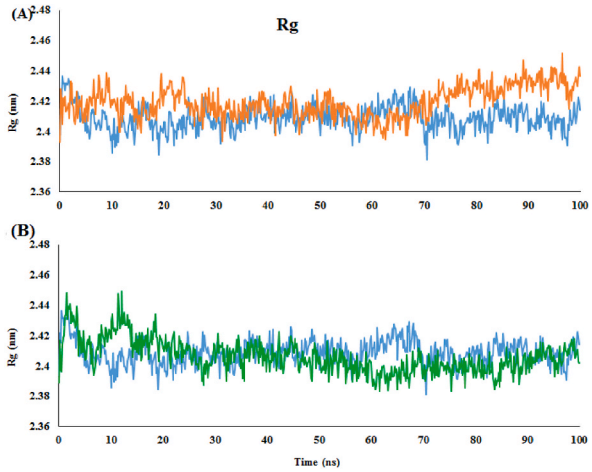


**Fig. 8.** Radius of gyration (Rg) graphs of **3b** (brown), **3c** (green), and acarbose (blue) complexes.

from 5ns to 100ns. Ligand **3b** exhibited a lower RMSD value than acarbose with large fluctuation (Fig. 6).

### *3.7. Root mean square fluctuation (RMSF)*

The RMSF value of the enzyme's amino acids was investigated to demonstrate the enzyme structure flexibility. Fig. 5 displays that the active site area was relatively rigid. The fluctuation of the active site for the **3b**-α-glucosidase complex is more significant, and the **3c**-α-glucosidase complex is smaller as compared to acarbose, which shows compound **3c** has strong interactions with active site residues and is stable in the active site. Analysis of the results from the **3b**-α-glucosidase revealed that this compound fluctuates to a greater degree. This proposes that the behavior of **3b** is not an effect of the protein conformation and is characteristic of the compound itself. Furthermore, Fig. 7 displays that derivative **3c** well fitted and firmly fastened the active site, which decreased the flexibility of the amino acids via interacting with main residues and resulted in the inhibition of α-glucosidase.

For example, in acarbose Phe303, Glu411, Glu277, Asp215, Tyr158, His112, Phe178, Phe159, Asp352, His351, Arg442, and Asn415 showed maximum RMSFs of 0.767, 0.608, 0.725, 0.562, 0.568, 0.564, 0.532, 0.582, 0.637, 0.601, 0.565 and 0.838 Å. About in compound **3c** Phe303, Glu411, Glu277, Asp215, Tyr158, His112, Phe178, Phe159, Asp352, His351, Arg442 and Asn415 showed maximum RMSFs of 0.709, 0.917, 0.699, 0.577, 0.566, 0.577, 0.518, 0.576, 0.579, 1.058 and 0.589 Å. In compound **3b** Phe303, Glu411, Glu277, Asp215, Tyr158, His112, Phe178, Phe159, Asp352, His351, Arg442, Asn415 showed maximum RMSFs of 0.812, 0.631, 0.480, 0.50, 0.729, 0.545, 0.603, 0.720, 0.624, 0.644, 0.634 and 1.199 Å. A comparison of all complexes RMSF results exhibited that, Asp215, Tyr158, His112, Phe178, Phe159 and Arg442 residues displayed the smallest fluctuation with acarbose as the drug standard. While, Asp215, Tyr158, His112, Phe178, Phe159, Asp352, His351 and Asn415 exhibited the smallest fluctuation with compound **3c**. Glu277, Asp215 and His112 displayed the smallest fluctuation with compound **3b**. According to the results, all compounds showed the smallest fluctuation with Asp215 and His112. Acarbose and compound **3c** showed strong interactions with Tyr158, Phe178, and Phe159, however, compound **3b** showed higher fluctuation with these residues. These observations correlated with docking results and previous studies [5].

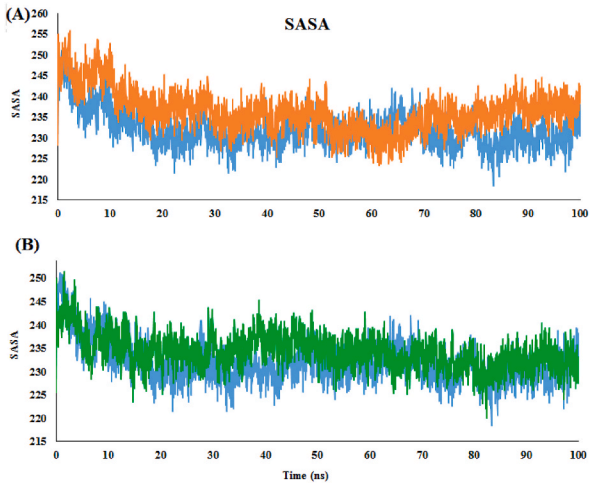


**Fig. 9.** SASA plot for α-glucosidase complexes of acarbose, compound **3c** and compound **3b** (shown in blue, green and brown, respectively).

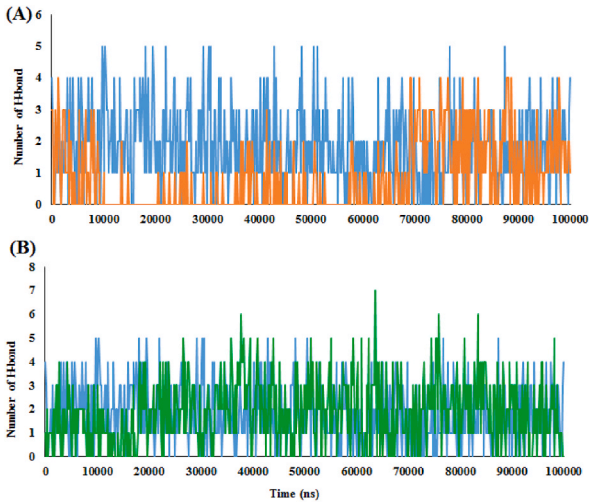


**Fig. 10.** Hydrogen bond numbers between α-glucosidase and compound **3c** (green), compound **3b** (brown) and acarbose (blue) over MD production run.

### *3.7.1. Radius of gyration (Rg)*

To know the compact of the enzyme, the radius of gyration (Rg) was investigated. The number of residues present in the enzyme is important in the Rg value [43]. When the protein structure has proper folding and stability, the Rg value is lower and stable. However, improper folding and conformational flexibility of the enzyme has a very fluctuating Rg value [44].

The average Rg values of acarbose-α-glucosidase, **3c**-α-glucosidase, and compound **3b**-α-glucosidase complexes were 2.41 nm, 2.42 nm, and 2.40 nm, respectively. The Rg value of the compound **3b**-α-glucosidase complex showed an increase after 70 ns however the Rg of acarbose-α-glucosidase dropped after 70ns. The **3c**-α-glucosidase complex exhibited more a constant Rg value during MD simulation; a minor lowering was detected from 2 to 2.35 ns then increasing was observed from 2.35 to 2.43 ns. A slight decrease again was detected from 2.43 to 3.7 ns (Fig. 8). The Rg value shows that the **3b**-α-glucosidase complex was fairly unstable toward the acarbose and compound **3c** because they accepted a more controlled conformation for the period of the simulation. Thus, the compound has less stability in the flap, and interactions between residues, and hinge domains are mainly affected.

### *3.7.2. Solvent accessible surface area (SASA)*

The surface area of a compound-enzyme complex that interacts with solvent molecules is accounted for by SASA. An open or extended enzyme structure exposed more to solvent shows higher SASA. The average SASA for the acarbose was 232.04 $nm^2$, while it was for compounds **3b** and **3c** 236.48 $nm^2$ and 234.27 $nm^2$, respectively. This funding shows solvent interaction with complexes was relatively similar and also confirms the residue flexibility and compactness analysis results. The SASA value slightly decreased for complexes and then it showed almost a constant SASA value throughout the simulation. Fluctuations were similar in very minor

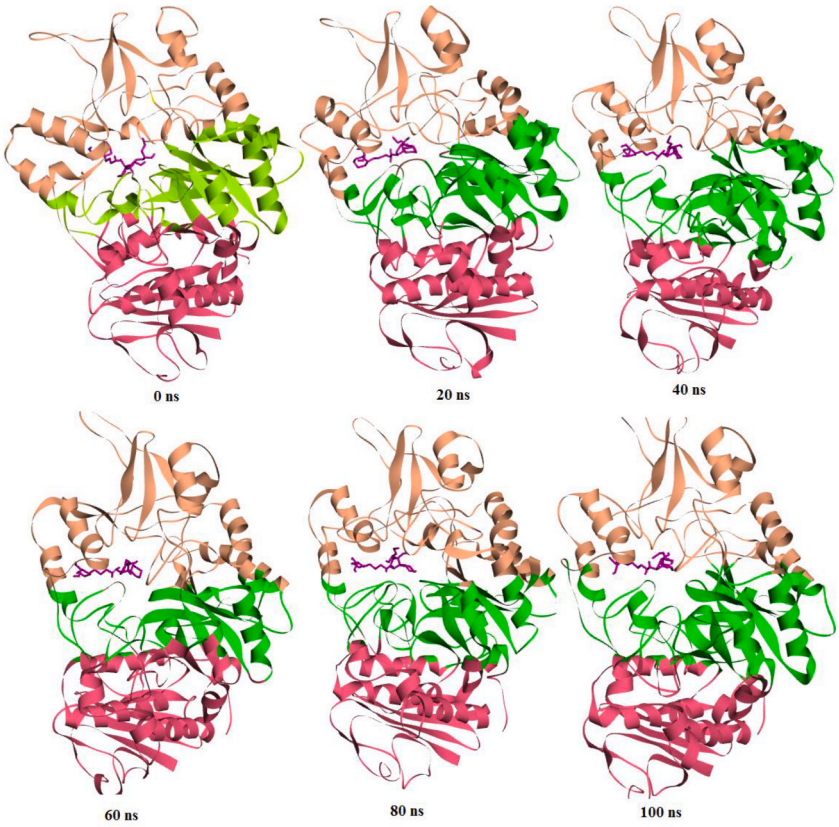


**Fig. 11.** Snapshots of compound **3c**-α-glucosidase complex at interval of every 20 ns of MD simulations.

complexes. Comparatively, the compound **3b**-α-glucosidase complex showed higher SASA suggesting less stability than the **3c**-α-glucosidase complex (Fig. 9).

### *3.7.3. Hydrogen bonding analysis*

One of the indicators of the binding stability of the compound-enzyme complex is the formation of hydrogen bonds between the compound and the enzyme. The MD findings exhibited intermolecular hydrogen bonds made significantly between compounds and amino acids (Fig. 10). The average hydrogen bonds for compounds **3c**, **3b**, and acarbose complexes are 1.86, 0.80, and 1.81, respectively. The hydrogen bonds of **3c**-α-glucosidase were higher compared to **3b** and acarbose complexes. However, the hydrogen bonds were constant throughout the simulation for compounds **3c** and **3b** complexes, indicating stronger binding between these compounds and α-glucosidase and leading to a highly stable conformation. The number of hydrogen bonds made throughout the simulations in compounds **3c** and **3b** was more than acarbose.

### *3.7.4. Structural analysis during MD simulations*

To understand the structural variations in **3c**-, **3b**-, and acarbose-α-glucosidase, the conformational snapshots at the distance of every 20 ns were taken overall 100 ns. In first 20 ns revealed more fluctuation for the **3c**-α-glucosidase complex but in the following, because of more compactness in the active site enzyme (reflected by Rg and SASA findings), the complex showed less structural variations and more stability from 40 ns to 100 ns (Fig. 11).

For compound **3b**-α-glucosidase complex snapshots were provided. In the first 20 ns, this complex showed more fluctuation; then, it exhibited high stability and less structural variations from 40 ns to 80 ns. Afterward, due to extension in the active site (reflected by SASA and Rg studies), the complex showed less stability and more structural variations from 80 ns to 100 ns (Fig. 12).

Moreover, the snapshots were achieved for acarbose-α-glucosidase. Acarbose demonstrated structural variations only for primary 40 ns and then kept almost constant until 100 ns (Fig. 13).

### *3.7.5. Binding free energy*

The MD/MM-PBSA affords diverse separate components, such as $\Delta E_{vdW}$, $\Delta E_{elec}$, $\Delta G_{pol}$, $\Delta G_{npol}$, and $T\Delta S$, to the total binding free energy ($\Delta G_{binding}$) (Table 2). It is obvious from Table 2 that $\Delta E_{elec}$ and $\Delta E_{vdW}$ preferred the binding, whereas $\Delta E_{npol}$ and $\Delta E_{pol}$ disfavored the complexation. For both cases, $\Delta E_{pol}$ is positive, which means that the electrostatic and van der Waals interactions chiefly determine the binding.

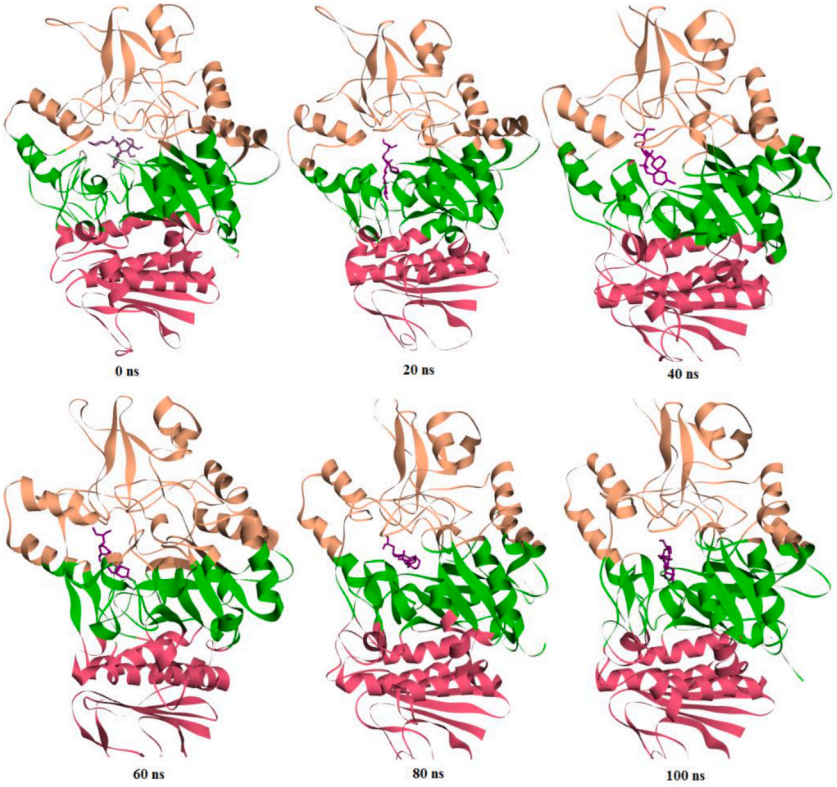


**Fig. 12.** Snapshots of compound **3b**-α-glucosidase complex at interval of every 20 ns of MD simulations.

Moreover, Table 2 exposes that the $\Delta G_{binding}$ of **3c** is higher (−260.950 kcal/mol) than **3b** (−222.452 kcal/mol). This can be because $\Delta E_{vdW}$ and $\Delta E_{elec}$ are more favorable in **3c**-α-glucosidase ($\Delta E_{vdW} = -57.730$ kcal/mol, $\Delta E_{elec} = -355.092$ kcal/mol) than **3b**-α-glucosidase ($\Delta E_{vdW} = -48.521$ kcal/mol, $\Delta E_{elec} = -308.575$ kcal/mol). Generally, this finding proposes that **3c** showed higher activity on α-glucosidase compared to **3b**.

Next, the binding affinity of compounds **3b** and **3c** were estimated and compared with acarbose. Acarbose showed binding energy lower (−159.271 kcal/mol) than **3b** and **3c** (Table 2). It is also displayed that the van der Waals interactions (−42.915 kcal/mol) unfavored the complex formation less compared to the electrostatic interaction (−226.624 kcal/mol). This is in approving with what has been detected for compounds **3b** and **3c**. This result showed that the binding affinity reduces in the following order against α-glucosidase: **3c** > **3b** > acarbose (Table 2).

After that, the binding free energy of the crucial amino acids involved in the compound-enzyme binding was analyzed with MM-PBSA. The MM-PBSA investigates hotspot amino acids in interaction energy which are higher than −1.0 kcal/mol (Table 3). According to Table 3, compound **3c** has interacted with a more significant number of crucial amino acids (Tyr72, Tyr158, Phe159, and Phe178) toward compound **3b** and acarbose. This can be one of the causes for the higher affinity and inhibitory activity of compound **3c** compared to compound **3b** against α-glucosidase (see Tables 4 and 5).

## 4. Conclusion

In summary, some of the 2-hydrazolyl-4-thiazolidinone hybrids were synthesized using a new route with more yield and fewer steps. All titled derivatives showed weak to good activity against α-glucosidase relative to acarbose as a drug. Two compounds **3b** and **3c** showed the highest inhibitory activity. Compound **3c** having a *para*-nitrophenyl ring and methyl ester moiety was the most potent one with an $IC_{50}$ value of 174 μM. A kinetic finding exhibited that **3c** inhibited via a competitive mechanism. Moreover, docking study and molecular dynamics simulations displayed that compound **3c** as the most potent compound was stable and fit in the active site and showed key interactions with vital residues compared to compound **3b** and acarbose.

## CRediT authorship contribution statement

**Saghi Sepehri:** Writing – review & editing, Writing – original draft, Supervision, Software, Project administration, Methodology, Investigation, Formal analysis, Data curation, Conceptualization. **Ghazaleh Farhadi:** Writing – original draft, Methodology, Investigation, Data curation. **Maryam Maghbul:** Writing – original draft, Methodology, Investigation. **Farough Nasiri:** Writing – review &

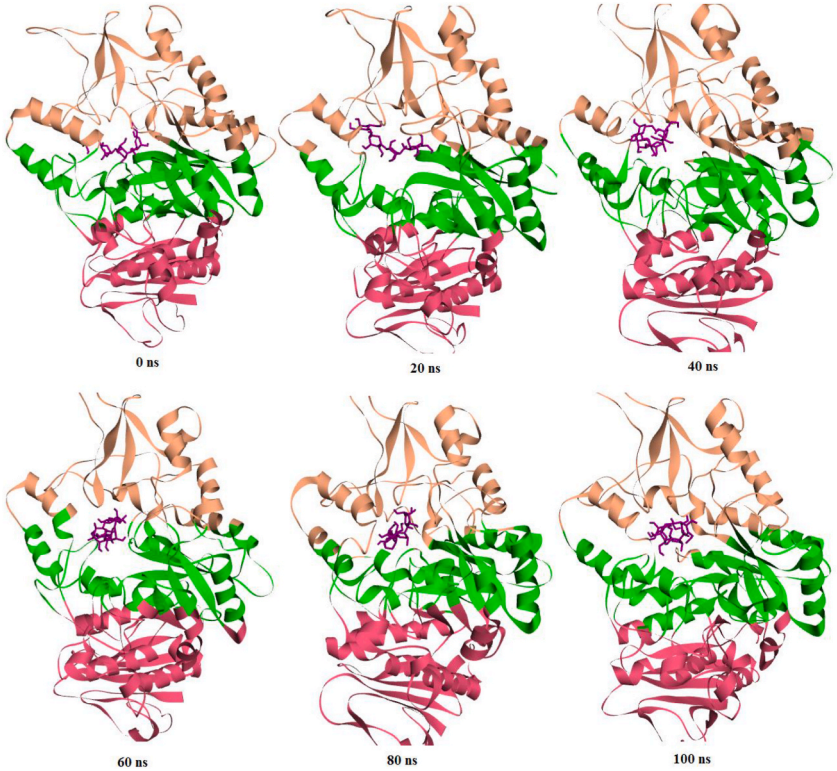


**Fig. 13.** Snapshots of acarbose-α-glucosidase complex at interval of every 10 ns of MD simulations.

**Table 2**
Molecular energy terms for interactions of two compounds and acarbose with α-glucosidase.

| Terms | Energy (kcal/mol) | | |
|---|---|---|---|
| | 3b | 3c | Acarbose |
| ΔEbinding | −222.452 | −260.950 | −159.271 |
| ΔEelec | −308.575 | −355.092 | −226.624 |
| ΔEvdW | −48.521 | −57.730 | −42.915 |
| ΔEpol | 110.132 | 123.521 | 73.328 |
| ΔEnpol | −24.009 | −29.379 | −19.643 |

**Table 3**
Interaction energy of hotspot residues considered with **3c**.

| Residues | $\Delta E_{binding}$ | $\Delta E_{MM}$ | $\Delta E_{pol}$ | $\Delta E_{npol}$ |
|---|---|---|---|---|
| Asp69 | −0.04 | −0.21 | 0.17 | −0.04 |
| Tyr72 | −8.03 | −11.54 | 4.33 | −0.85 |
| His112 | −0.90 | −1.88 | 1.03 | −0.04 |
| Lys156 | 6.41 | −5.64 | 12.52 | −0.49 |
| Tyr158 | −15.18 | −17.98 | 4.14 | −1.31 |
| Phe159 | −14.34 | −15.17 | 1.75 | −0.94 |
| Phe178 | −11.66 | −14.00 | 3.45 | −1.01 |
| Arg213 | −0.14 | 0.08 | −0.20 | 0 |
| Asp215 | 0.56 | 0.13 | 0.42 | 0 |

editing, Writing – original draft, Supervision, Methodology, Investigation, Data curation, Conceptualization. **Mohammad Ali Faramarzi:** Writing – original draft, Supervision, Methodology, Investigation. **Karim Mahnam:** Methodology, Investigation, Formal analysis, Data curation, Conceptualization. **Somayeh Mojtabavi:** Methodology, Investigation, Formal analysis. **Mohammad Mahdavi:** Supervision, Methodology, Investigation, Formal analysis, Data curation, Conceptualization. **Zhaleh Moharrami Oranj:** Methodology, Formal analysis.

**Table 4**
Interaction energy of hotspot residues considered with **3b**.

| Residues | $\Delta E_{binding}$ | $\Delta E_{MM}$ | $\Delta E_{pol}$ | $\Delta E_{npol}$ |
|---|---|---|---|---|
| Asp69 | −0.43 | −0.31 | −0.12 | 0 |
| Tyr72 | −0.41 | −0.49 | 0.10 | −0.02 |
| His112 | −1.93 | −6.04 | 4.44 | −0.33 |
| Lys156 | 8.45 | −2.00 | 10.59 | −0.06 |
| Tyr158 | −10.06 | −12.61 | 3.24 | −0.69 |
| Phe159 | −15.31 | −16.52 | 1.98 | −0.79 |
| Phe178 | −5.42 | −7.51 | 2.62 | −0.55 |
| Arg213 | −0.76 | −2.07 | 1.30 | 0 |
| Asp215 | 3.02 | 5.13 | −2.15 | −0.01 |

**Table 5**
Interaction energy of hotspot residues considered with acarbose.

| Residues | $\Delta E_{binding}$ | $\Delta E_{MM}$ | $\Delta E_{pol}$ | $\Delta E_{npol}$ |
|---|---|---|---|---|
| Asp69 | −0.38 | −0.22 | −0.15 | 0 |
| Tyr72 | 0.01 | −0.12 | 0.12 | 0 |
| His112 | 0.07 | 0.05 | 0.02 | 0 |
| Lys156 | 2.87 | −3.94 | 6.85 | −0.08 |
| Tyr158 | −7.61 | −12.26 | 5.46 | −0.88 |
| Phe159 | −4.07 | −4.61 | 0.92 | −0.41 |
| Phe178 | −0.98 | −1.06 | 0.19 | −0.12 |
| Arg213 | 1.39 | 1.62 | −0.21 | 0 |
| Asp215 | −1.40 | −1.06 | −0.35 | 0 |

## Declaration of competing interest

The authors declare the following financial interests/personal relationships which may be considered as potential competing interests:Saghi Sepehri reports financial support was provided by Ardabil University of Medical Sciences. If there are other authors, they declare that they have no known competing financial interests or personal relationships that could have appeared to influence the work reported in this paper.

## Acknowledgements

This research was supported by Ardabil University of Medical Sciences. Funding Number is IR.ARUMS.REC.1401.241.

## Appendix A. Supplementary data

Supplementary data to this article can be found online at https://doi.org/10.1016/j.heliyon.2024.e36408.

## References

[1] L. Chen, Z. Jiang, L. Yang, Y. Fang, S. Lu, O.U. Akakuru, S. Huang, J. Li, S. Ma, A. Wu, HPDA/Zn as a CREB inhibitor for ultrasound imaging and stabilization of atherosclerosis plaque, Chin. J. Chem. 41 (2023) 199–206.
[2] Y. Zhou, X. Chai, G. Yang, X. Sun, Z. Xing, Changes in body mass index and waist circumference and heart failure in type 2 diabetes mellitus, Front. Endocrinol. 14 (2023).
[3] D. Liang, X. Cai, Q. Guan, Y. Ou, X. Zheng, X. Lin, Burden of type 1 and type 2 diabetes and high fasting plasma glucose in Europe, 1990-2019: a comprehensive analysis from the global burden of disease study 2019, Front. Endocrinol. 14 (2023).
[4] Y. Yu, L. Wang, S. Ni, D. Li, J. Liu, H.Y. Chu, N. Zhang, M. Sun, N. Li, Q. Ren, Z. Zhuo, C. Zhong, D. Xie, Y. Li, Z.-K. Zhang, H. Zhang, M. Li, Z. Zhang, L. Chen, X. Pan, W. Xia, S. Zhang, A. Lu, B.-T. Zhang, G. Zhang, Targeting loop3 of sclerostin preserves its cardiovascular protective action and promotes bone formation, Nat. Commun. 13 (2022) 4241.
[5] Z. Bakherad, H. Bakherad, S. Sepehri, M.A. Faramarzi, K. Mahnam, S. Mojtabavi, M. Mahdavi, In silico and in vitro studies of thiosemicarbazone-indole hybrid compounds as potent α-glycosidase inhibitors, Comput. Biol. Chem. 97 (2022) 107642.
[6] S.R. Joshi, E. Standl, N. Tong, P. Shah, S. Kalra, R. Rathod, Therapeutic potential of α-glucosidase inhibitors in type 2 diabetes mellitus: an evidence-based review, Expet Opin. Pharmacother. 16 (2015) 1959–1981.
[7] C. Proença, M. Freitas, D. Ribeiro, E.F.T. Oliveira, J.L.C. Sousa, S.M. Tomé, M.J. Ramos, A.M.S. Silva, P.A. Fernandes, E. Fernandes, α-Glucosidase inhibition by flavonoids: an in vitro and in silico structure-activity relationship study, J. Enzym. Inhib. Med. Chem. 32 (2017) 1216–1228.
[8] E.U. Mughal, M.B. Hawsawi, N. Naeem, A. Hassan, M.S. Alluhaibi, S.W. Ali Shah, Y. Nazir, A. Sadiq, H.A. Alrafai, S.A. Ahmed, Exploring fluorine-substituted piperidines as potential therapeutics for diabetes mellitus and Alzheimer's diseases, Eur. J. Med. Chem. 273 (2024) 116523.
[9] M. Karami, A. Hasaninejad, H. Mahdavi, A. Iraji, S. Mojtabavi, M.A. Faramarzi, M. Mahdavi, One-pot multi-component synthesis of novel chromeno[4,3-b] pyrrol-3-yl derivatives as alpha-glucosidase inhibitors, Mol. Divers. 26 (2022) 2393–2405.

[10] J. Ren, J. Dai, Y. Chen, Z. Wang, R. Sha, J. Mao, Physiochemical characterization and ameliorative effect of rice resistant starch modified by heat-stable α-amylase and glucoamylase on the gut microbial community in T2DM mice, Food Funct. 15 (2024) 5596–5612.
[11] N.B. Patel, F.M. Shaikh, Synthesis and antimicrobial activity of new 4-thiazolidinone derivatives containing 2-amino-6-methoxybenzothiazole, Saudi Pharmaceut. J. : SPJ : the official publication of the Saudi Pharmaceutical Society 18 (2010) 129–136.
[12] P. Prieto, M. Pineda, M. Aguilar, Spectrophotometric quantitation of antioxidant capacity through the formation of a phosphomolybdenum complex: specific application to the determination of vitamin E, Anal. Biochem. 269 (1999) 337–341.
[13] M.G. Vigorita, R. Ottanà, F. Monforte, R. Maccari, A. Trovato, M.T. Monforte, M.F. Taviano, Synthesis and antiinflammatory, analgesic activity of 3,3′-(1,2-Ethanediyl)-bis[2-aryl-4-thiazolidinone] chiral compounds. Part 10, Bioorg. Med. Chem. Lett 11 (2001) 2791–2794.
[14] S. Bouzroura, Y. Bentarzi, R. Kaoua, B.N.-K.S. Poulain-Martini, E. Dunach, A convenient one pot preparation of 4-thiazolidinones from enaminolactones, Org. Commun. 3 (2010) 8.
[15] D. Crowfoot, C.W. Bunn, B.W. Rogers-Low, A. Turner-Jones, The X-ray crystallographic investigation of the structure of penicillin, Chemistry of penicillin (1949) 310–367.
[16] Z. Hussain, A. Mahmood, Q. Shah, A. Imran, E.U. Mughal, W. Khan, A. Baig, J. Iqbal, A. Mumtaz, Synthesis and evaluation of amide and thiourea derivatives as carbonic anhydrase (CA) inhibitors, ACS Omega 7 (2022) 47251–47264.
[17] H. Ullah, I. Uddin, F. Rahim, F. Khan, Sobia, M. Taha, M.U. Khan, S. Hayat, M. Ullah, Z. Gul, S. Ullah, H. Zada, J. Hussain, In vitro α-glucosidase and α-amylase inhibitory potential and molecular docking studies of benzohydrazide based imines and thiazolidine-4-one derivatives, J. Mol. Struct. 1251 (2022) 132058.
[18] S.A. Khan, M. Ali, A. Latif, M. Ahmad, A. Khan, A. Al-Harrasi, Mercaptobenzimidazole-based 1, 3-Thaizolidin-4-ones as antidiabetic agents: synthesis, in vitro α-glucosidase inhibition activity, and molecular docking studies, ACS Omega 7 (2022) 28041–28051.
[19] K. Szabó, R. Maccari, R. Ottanà, G. Gyémánt, Extending the investigation of 4-thiazolidinone derivatives as potential multi-target ligands of enzymes involved in diabetes mellitus and its long-term complications: a study with pancreatic α-amylase, Carbohydr. Res. 499 (2021) 108220.
[20] M.J. Nanjan, M. Mohammed, B.R. Prashantha Kumar, M.J.N. Chandrasekar, Thiazolidinediones as antidiabetic agents: a critical review, Bioorg. Chem. 77 (2018) 548–567.
[21] Aisha, M.A. Raza, S.H. Sumrra, K. Javed, Z. Saqib, J.K. Maurin, A. Budzianowski, Synthesis, characterization and molecular modeling of amino derived thiazolidinones as esterase and glucosidase inhibitors, J. Mol. Struct. 1219 (2020) 128609.
[22] S.A. Khan, M. Ali, A. Latif, M. Ahmad, A. Khan, A. Al-Harrasi, Mercaptobenzimidazole-based 1,3-Thaizolidin-4-ones as antidiabetic agents: synthesis, in vitro α-glucosidase inhibition activity, and molecular docking studies, ACS Omega 7 (2022) 28041–28051.
[23] S. Khan, S. Iqbal, F. Rahim, M. Shah, R. Hussain, H. Alrbyawi, W. Rehman, A.A. Dera, L. Rasheed, H.H. Somaily, R.A. Pashameah, E. Alzahrani, A.E. Farouk, New biologically hybrid pharmacophore thiazolidinone-based indole derivatives: synthesis, in vitro αlpha-amylase and αlpha-glucosidase along with molecular docking investigations, Molecules 27 (2022).
[24] Y. Chinthala, A. Kumar Domatti, A. Sarfaraz, S.P. Singh, N. Kumar Arigari, N. Gupta, S.K. Satya, J. Kotesh Kumar, F. Khan, A.K. Tiwari, G. Paramjit, Synthesis, biological evaluation and molecular modeling studies of some novel thiazolidinediones with triazole ring, Eur. J. Med. Chem. 70 (2013) 308–314.
[25] A.V. Shastin, V.N. Korotchenko, V.G. Nenajdenko, E.S. Balenkova, A novel synthetic approach to dichlorostyrenes, Tetrahedron 56 (2000) 6557–6563.
[26] M. Adib, F. Peytam, M. Rahmanian-Jazi, M. Mohammadi-Khanaposhtani, S. Mahernia, H.R. Bijanzadeh, M. Jahani, S. Imanparast, M.A. Faramarzi, M. Mahdavi, Design, synthesis and in vitro α-glucosidase inhibition of novel coumarin-pyridines as potent antidiabetic agents, New J. Chem. 42 (2018) 17268–17278.
[27] A. Keivanloo, S. Sepehri, M. Bakherad, M. Eskandari, Click synthesis of 1,2,3-triazoles-linked 1,2,4-Triazino[5,6-b]indole, antibacterial activities and molecular docking studies, ChemistrySelect 5 (2020) 4091–4098.
[28] N. Razzaghi-Asl, S. Mirzayi, K. Mahnam, V. Adhami, S. Sepehri, In silico screening and molecular dynamics simulations toward new human papillomavirus 16 type inhibitors, Res Pharm Sci 17 (2022) 189–208.
[29] A. Saeed, N.A. Al-Masoudi, M. Latif, Synthesis and antiviral activity of new substituted methyl [2-(arylmethylene-hydrazino)-4-oxo-thiazolidin-5-ylidene] acetates, Arch. Pharmazie 346 (2013) 618–625.
[30] C. Pizzo, C. Saiz, A. Talevi, L. Gavernet, P. Palestro, C. Bellera, L.B. Blanch, D. Benítez, J.J. Cazzulo, A. Chidichimo, P. Wipf, S.G. Mahler, Synthesis of 2-hydrazolyl-4-thiazolidinones based on multicomponent reactions and biological evaluation against Trypanosoma Cruzi, Chem. Biol. Drug Des. 77 (2011) 166–172.
[31] A. Benmohammed, O. Khoumeri, A. Djafri, T. Terme, P. Vanelle, Synthesis of novel highly functionalized 4-thiazolidinone derivatives from 4-phenyl-3-thiosemicarbazones, Molecules 19 (2014) 3068–3083.
[32] Y.-Y. Yang, Z. Chen, X.-D. Yang, R.-R. Deng, L.-X. Shi, L.-Y. Yao, D.-X. Xiang, Piperazine ferulate prevents high-glucose-induced filtration barrier injury of glomerular endothelial cells, Exp. Ther. Med. 22 (2021) 1175.
[33] J.M. Li, X. Li, L.W.C. Chan, R. Hu, T. Zheng, H. Li, S. Yang, Lipotoxicity-polarised macrophage-derived exosomes regulate mitochondrial fitness through Miro1-mediated mitophagy inhibition and contribute to type 2 diabetes development in mice, Diabetologia 66 (2023) 2368–2386.
[34] L. Xu, T. Wang, Y. Shan, R. Wang, C. Yi, Soybean protein isolate inhibiting the retrogradation of fresh rice noodles: combined experimental analysis and molecular dynamics simulation, Food Hydrocolloids 151 (2024) 109877.
[35] X. Li, J. Liang, J. Hu, L. Ma, J. Yang, A. Zhang, Y. Jing, Y. Song, Y. Yang, Z. Feng, Screening for primary aldosteronism on and off interfering medications, Endocrine 83 (2024) 178–187.
[36] S. Cheng, M. Huang, S. Liu, M. Yang, Bisphenol F and bisphenol S induce metabolic perturbations in human ovarian granulosa cells, Arab. J. Chem. (2024) 105904.
[37] Q. Wang, Q. Guo, W. Niu, L. Wu, W. Gong, S. Yan, K. Nishinari, M. Zhao, The pH-responsive phase separation of type-A gelatin and dextran characterized with static multiple light scattering (S-MLS), Food Hydrocolloids 127 (2022) 107503.
[38] N. Shayegan, S. Haghipour, N. Tanideh, A. Moazzam, S. Mojtabavi, M.A. Faramarzi, C. Irajie, S. Parizad, S. Ansari, B. Larijani, S. Hosseini, A. Iraji, M. Mahdavi, Synthesis, in vitro α-glucosidase inhibitory activities, and molecular dynamic simulations of novel 4-hydroxyquinolinone-hydrazones as potential antidiabetic agents, Sci. Rep. 13 (2023) 6304.
[39] M. Mohammadi-Khanaposhtani, S. Rezaei, R. Khalifeh, S. Imanparast, M.A. Faramarzi, S. Bahadorikhalili, M. Safavi, F. Bandarian, E. Nasli Esfahani, M. Mahdavi, B. Larijani, Design, synthesis, docking study, α-glucosidase inhibition, and cytotoxic activities of acridine linked to thioacetamides as novel agents in treatment of type 2 diabetes, Bioorg. Chem. 80 (2018) 288–295.
[40] T. Ernawati, In silico evaluation of molecular interactions between known α-glucosidase inhibitors and homologous α-glucosidase enzymes from Saccharomyces cerevisiae, Rattus norvegicus, and GANC-human, Thai Journal of Pharmaceutical Sciences (TJPS) (2018) 42.
[41] H. Sun, W. Ding, X. Song, D. Wang, M. Chen, K. Wang, Y. Zhang, P. Yuan, Y. Ma, R. Wang, R.H. Dodd, Y. Zhang, K. Lu, P. Yu, Synthesis of 6-hydroxyaurone analogues and evaluation of their α-glucosidase inhibitory and glucose consumption-promoting activity: development of highly active 5,6-disubstituted derivatives, Bioorg. Med. Chem. Lett 27 (2017) 3226–3230.
[42] N. Ahangarzadeh, N. Shakour, S. Rezvanpoor, H. Bakherad, M.H. Pakdel, G. Farhadi, S. Sepehri, Design, synthesis, and in silico studies of tetrahydropyrimidine analogs as urease enzyme inhibitors, Arch. Pharmazie (2022) e2200158.
[43] M. Sivakumar, K. Saravanan, V. Saravanan, S. Sugarthi, S.M. Kumar, M. Alhaji Isa, P. Rajakumar, S. Aravindhan, Discovery of new potential triplet acting inhibitor for Alzheimer's disease via X-ray crystallography, molecular docking and molecular dynamics, J. Biomol. Struct. Dynam. 38 (2020) 1903–1917.
[44] R. Biswas, N. Chowdhury, R. Mukherjee, A. Bagchi, Identification and analyses of natural compounds as potential inhibitors of TRAF6-Basigin interactions in melanoma using structure-based virtual screening and molecular dynamics simulations, J. Mol. Graph. Model. 85 (2018) 281–293.